Numerical solution of the time-dependent Schrödinger equation in one dimension

Bernardine Renaldo Wong
Quantum Scattering Theory Group, Institute of Mathematical Sciences, University of Malaya, 50603 Kuala Lumpur, Malaysia

(Received 27 September 2006)

We implement a method to numerically solve the Time-Dependent Schrödinger Equation (TDSE) in one dimension. The time-dependence is modeled using the Crank-Nicholson formula. The discrete transparent boundary conditions are employed using a Numerov approximation formula. Preliminary results will be presented.

I. INTRODUCTION

The time-dependent Schrödinger equation (TDSE) is the fundamental equation of non-relativistic quantum mechanics. Since its postulation in 1926, the Schrödinger equation has found widespread application in many fields of physical science, for example in atomic, molecular, optical, nuclear and solid-state physics, among others. Unfortunately, the exact analytic solutions of the TDSE have been found for relatively few cases of interaction potentials.

In the special case of a time-independent potential function, $V(x)$, the solution of the TDSE may be written as a linear superposition of stationary states. These states (and their corresponding eigen-energies) can be obtained numerically (in general) by solving the time-independent Schrödinger equation (TISE). Given the initial wave-function it is possible to construct the wave-function at any general time from the linear superposition of, in principle, an infinite number of stationary states. On the other hand, due to the availability of high-speed computers, it is becoming possible to directly solve the TDSE. In this paper, we implement a method [1] to numerically solve the TDSE within a finite domain, whose boundaries obey transparent boundary conditions.

II. DIRECT APPROACH IN SOLVING THE TIME-DEPENDENT SCHRÖDINGER EQUATION

The TDSE, in one dimension, is expressed mathematically by

$$i\hbar \frac{\partial}{\partial t}\Psi(x,t) = H\,\Psi(x,t). \tag{1}$$

Here, $\hbar$ is the reduced Planck constant and $i=\sqrt{-1}$. The Hamiltonian operator is

$$H = \left[-\frac{\hbar^2}{2m}\frac{\partial^2}{\partial x^2} + V(x,t) \right]. \tag{2}$$

The wave-function $\Psi(x,t)$ gives the probability amplitude for representing the state of a particle of mass m moving under the action of forces described by a potential energy function, Here, it is assumed that the wave-function will vanish if the position $x \to \pm\infty$ at any time $t > 0$. In practice, the TDSE is solved only within a sub-domain $\{x, t \in \Re | x_L \le x \le x_R, t > 0\}$. Here, x_L and x_R denote the left- and the right-endpoints, respectively. Let the spatial interval $[x_L, x_R]$ be sub-divided by $M+1$ equidistant points at intervals of step-size Δx. Hence, we create the spatial grid $x_L = x_0, x_1, \ldots, x_M = x_R$. In a similar manner, the time evolution can be discretized in time-steps of Δt. In order to numerically calculate the value of the wave-function at the specified grid points in space-time, we use the formal solution of the TDSE, which is,

$$\Psi(x, t+\Delta t) = e^{-(i\Delta t/\hbar)H}\Psi(x,t), \tag{3}$$

where H is the Hamiltonian operator. Goldberg *et al.* [2] used the approximation

$$e^{-(i\Delta t/\hbar)H} = \frac{1-(i\Delta t/2\hbar)H}{1+(i\Delta t/2\hbar)H} + O((H\Delta t)^3), \tag{4}$$

such that, on substitution in Eq. (3), the solution at time $t+\Delta t$ (denoted by Ψ_j^{n+1}) can be obtained from the solution at time t (denoted by Ψ_j^n) according to the formula

$$\left(1+\frac{i\Delta t}{2\hbar}H\right)\Psi_j^{n+1} = \left(1-\frac{i\Delta t}{2\hbar}H\right)\Psi_j^n. \tag{5}$$

This Crank-Nicholson algorithm [3] requires only the initial wave-function to generate the wave-function at subsequent times. In addition, it is unconditionally stable and unitary, implying that the wave-function normalization is preserved. However, from a

computational viewpoint, the method is implicit and requires matrix inversions. Furthermore, the accuracy of the wave-function generated is limited by the errors in the spatial and temporal time-steps; for example, the error in the time propagation is of order $(\Delta t)^2$. In Goldberg *et al.* [2], the second-order spatial derivative appearing in H is approximated by centered-difference formula

$$\frac{\partial^2}{\partial x^2}\Psi_j^n = \frac{1}{(\Delta x)^2}\left[\Psi_{j+1}^n - 2\Psi_j^n + \Psi_{j-1}^n\right] + O((\Delta x)^2). \qquad (6)$$

Moyer [1] has recently found a way to implement the Numerov extension in the centered-difference formula which improves its accuracy from order $(\Delta x)^3$ to $(\Delta x)^5$. By defining the following quantities

$$g_j = \frac{2m}{\hbar^2}V_j - i\frac{4m}{\hbar(\Delta t)}, \qquad (7a)$$

$$d_j = 1 - \frac{(\Delta x)^2}{12}g_j, \qquad (7b)$$

$$f_j^n = i\frac{8m}{\hbar(\Delta t)}\Psi_j^n, \qquad (7c)$$

$$w_j^n = d_j\left(\Psi_j^{n+1} + \Psi_j^n\right) - \frac{(\Delta x)^2}{12}f_j^n, \qquad (7d)$$

$$a_j = 1 + \frac{(\Delta x)^2}{2d_j}g_j, \qquad (7e)$$

$$c_j = 1 - \frac{i(\Delta x)^2}{3d_j(\Delta t)}, \qquad (7f)$$

the finite-difference equation connecting the spatial variables takes the form

$$w_{j+1}^n + w_{j-1}^n = \left(2 + (\Delta x)^2\frac{g_j}{d_j}\right)w_j^n + (\Delta x)^2\frac{f_j^n}{d_j} + O((\Delta x)^6). \qquad (8)$$

Eq. (8), which incorporates the Numerov extension, reduces to that of the centered-difference approximation, (with an error term of order $(\Delta x)^2$), if we were to set $d_j = 1$ and $w_j^n = \Psi_j^{n+1} + \Psi_j^n$ in Eqs. (7b) and (7d), respectively.

Goldberg *et al.* [2] have also shown that the three-term recurrence, Eq. (8), can be reduced to a pair of two-term recurrence equations involving two new functions e_j and q_j^n satisfying the condition $w_{j+1}^n = e_j w_j^n + q_j^n$ for all intermediate spatial points, specified by indices $j = 1, 2, \ldots, M-1$. Eq. (8) can then be replaced by

$$e_j + \frac{1}{e_{j-1}} = 2 + (\Delta x)^2\frac{g_j}{d_j}, \qquad (9a)$$

$$q_j^n = \frac{q_{j-1}^n}{e_{j-1}} + (\Delta x)^2\frac{f_j^n}{d_j}. \qquad (9b)$$

Once e_j and q_j^n are known, we can use $w_{j-1}^n = (w_j^n - q_{j-1}^n)/e_{j-1}$ to determine $w_{M-1}^n, w_{M-2}^n, \ldots, w_1^n$. Once w_j^n has been found for all spatial points at time-step n, the discretized wave-function at time-step $n+1$ can be found by using

$$\Psi_j^{n+1} = -\Psi_j^n + i\frac{(\Delta x)^2}{3\Delta t}\frac{\Psi_j^n}{d_j} + \frac{w_j^n}{d_j}. \qquad (10)$$

In order to generate e_j and q_j^n for $j = 1, 2, \ldots, M-1$, boundary conditions have to be imposed. Moyer [1] has treated two cases: The rigid-wall boundary conditions require that $w_0^n = w_M^n = 0$ at all times. For the rigid wall boundary conditions, one is free to set a very large positive value for e_0 which allows one to calculate e_j and q_j^n.

On the other hand, Ehrhardt [5] and Ehrhardt and Arnold [6] and co-workers [7] have recently successfully implemented transparent boundary conditions which, when applied to the left endpoint, allow us to compute $w_1^n = \alpha_0 w_0^n + \beta_0^n$. Here, α_0 and β_0^n are

$$\alpha_0 = e_0 = a_0 \pm \sqrt{a_0^2 - 1}, \qquad (11a)$$

$$\beta_0^n = q_0^n = d_0^*(a_0^* - \alpha_0)\Psi_0^n + d_0(a_0 - \alpha_0)\sum_{k=1}^{n}\ell_{n-k+1}\Psi_0^k. \qquad (11b)$$

Here, the asterisks denote complex conjugation. Similarly, the transparent boundary condition applied to the right hand boundary allows us to compute $w_{J-1}^n = \alpha_J w_J^n + \beta_J^n$, where α_J and β_J^n are defined by

$$\alpha_J = a_J \pm \sqrt{a_J^2 - 1}, \qquad (12a)$$

$$\beta_M^n = d_M^*(a_M^* - \alpha_M)\Psi_M^n + d_M(a_M - \alpha_M)\sum_{k=1}^{n}\ell_{n-k+1}\Psi_M^k. \qquad (12b)$$

The ambiguity in the signs appearing in Eqs. (11a) and (12a) is resolved by requiring that $|\alpha_0|>1$ and $|\alpha_M|>1$, respectively. The coefficients ℓ_n are defined by

$$\ell_n = \frac{e^{-in\phi}}{2n-1}\left[P_n(\mu) - P_{n-2}(\mu)\right]. \tag{13}$$

Here, *P* refers to the Legendre polynomial of order *n* while its argument is

$$\mu_j = \frac{1-|a_j|^2}{|1-a_j^2|} \tag{14a}$$

and

$$\varphi_j = \arg[(a_j^2-1)/c_j]. \tag{14b}$$

The approach by Moyer [1] is an explicit method and computationally very efficient and accurate. It is beginning to be used widely; for example, see Veenstra *et al.* [4]. Using Eq. (10), numerical solutions of the TDSE can be computed at discrete points within the sub-domain $x_L \le x \le x_R$. If rigid wall boundary conditions are employed, one would need to use as wide an interval as possible, within the constraints of the available computing resources, to minimize the problem of spurious reflected waves from the boundaries of the spatial integration regions. However, with the transparent boundary condition approach of Ehrhardt and Arnold [6] as given in Eqs. (11)–(14), the zero-boundary conditions at infinity can be transformed into the transparent boundary conditions at x_L and x_R, dispensing with the presence of spurious reflections.

III. RESULTS OF CALCULATION AND DISCUSSION

We have implemented the Numerov method as given by equation (10) to both the rigid-wall and transparent boundary conditions. In the calculations below, we set $\hbar = 1$ and $m = 1/2$. We consider the wave-function at time $t = 0$ to be of Gaussian form

$$\Psi(x,0) = e^{ik_0 x}\, e^{-(x-x_0)^2/(2\sigma^2)} \tag{15}$$

which is centered about $x_0 = 0.5$ and with width $\sigma = 0.0625$. The wave number is $k_0 = 50$. The wave-function is then propagated in a field-free region using Eq. (10) by applying (i) rigid-wall, and (ii) transparent boundary conditions. Snapshots of the propagation of the absolute value of the wave-function $|\Psi(x,t)|$ at various times are shown in Fig. 1 below.

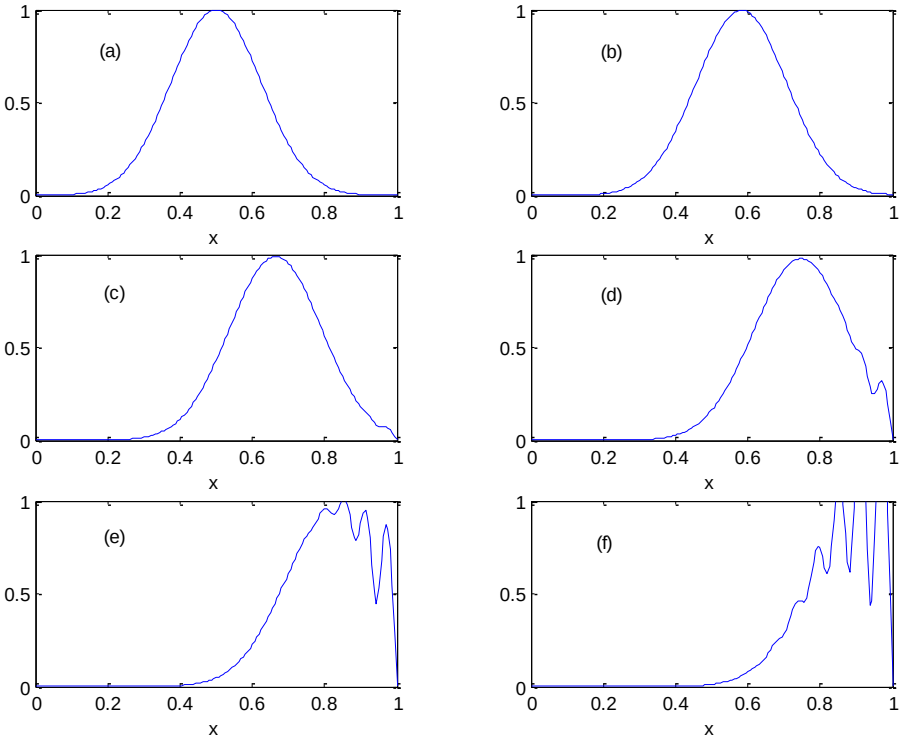

FIG. 1. Snapshots showing the propagation of the absolute value of the wave-function subject to rigid-wall boundary conditions at times (a) 0.0, (b) 0.001, (c) 0.002, (d) 0.003, (d) 0.004 and (e) 0.005.

In Figs. 1(c)–1(f), the wave-packet encounters the right endpoint. Imposition of rigid-wall boundary conditions causes spurious reflected waves to be generated. On the other hand, application of the transparent boundary conditions, Eqs. (11)–(14), allows for the propagation of the wave-packet beyond the right endpoint without any unphysical reflections, as demonstrated in Fig. 2 below.

As a second illustration of the transparent boundary conditions, we consider the propagation of the Gaussian wave-packet, Eq. (15), across a region with a double potential barrier which is defined by

$$V(x)=\begin{cases}0.0, & x<-7.5\\ 0.25 & -7.5\le x\le -2.5\\ 0.0, & -2.5\le x\le 2.5\\ 0.25, & 2.5\le x\le 7.5\\ 0.0, & x>7.5\end{cases}. \qquad (16)$$

Here, the initial wave-packet is centered about $x_0=-25.0$ and has a width $\sigma=3.162$. The wave number is $k_0=0.4$. Fig. 3 below shows the propagation of the initial wave-packet from left to right. The wave-packet encounters the double barrier potential, cf. Fig. 3(b), and is subsequently split into three parts comprising of a reflected wave, a transmitted wave and a standing wave which is confined between the barriers.

Therefore, Figs. 2 and 3 above show that Eq. (10) can be used to accurately propagate the wave-function. As the wave-function approaches the right boundary, the fixed-wall boundary condition leads to the formation of spurious reflections as seen in Fig. 1. If one wishes to avoid these reflections while retaining the fixed-wall boundary condition, it would be necessary to considerably widen the region. On the other hand, the use of the transparent boundary conditions, i.e. Eqs. (11)–(14), allows the propagation of the wave function without any spurious reflection at the boundary as seen in Figs. 2 and 3. Hence, one can simulate the propagation of a wave-function without unnecessarily broadening the region by using the transparent boundary condition approach.

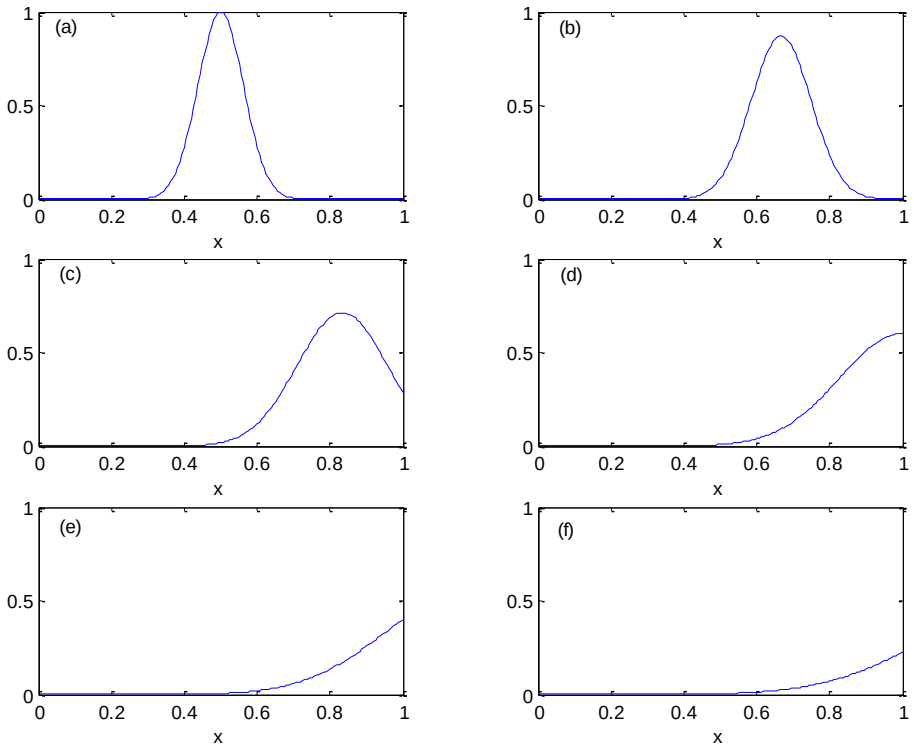

FIG. 2. Snapshots showing the propagation of the absolute value of the wave-function subject to transparent boundary conditions at times (a) 0.0, (b) 0.001, (c) 0.002, (d) 0.003, (d) 0.004 and (e) 0.005.

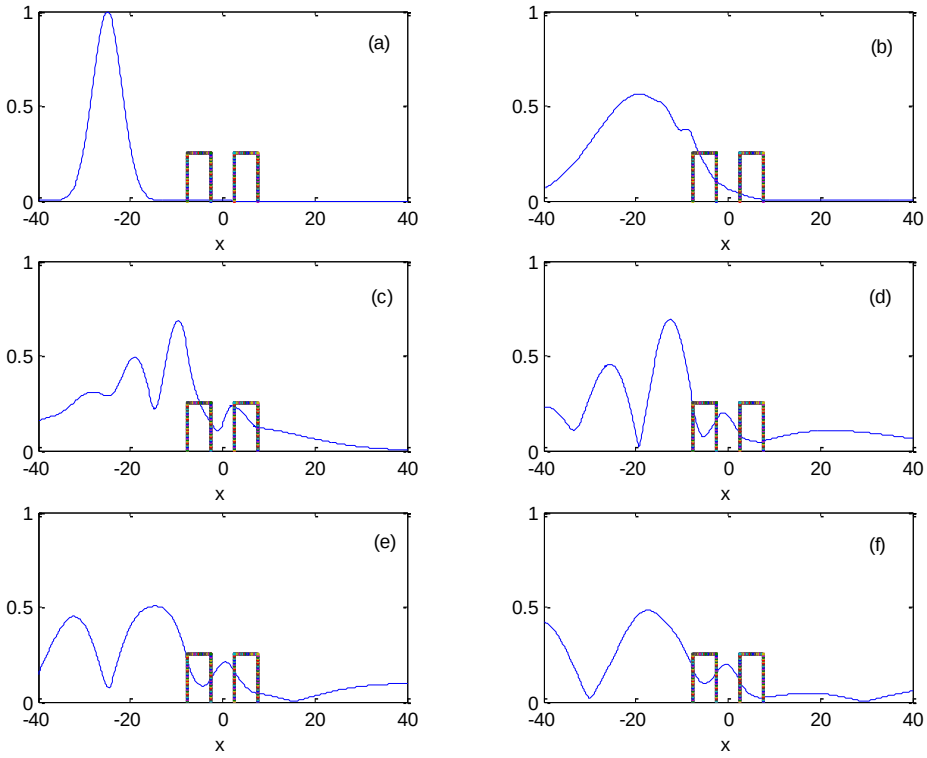

FIG. 3. Snapshots showing the propagation of the absolute value of the wave-function subject to transparent boundary conditions at times (a) 0.0, (b) 15.0, (c) 30.0, (d) 45.0, (d 60.0 and (e) 75.0.

IV. CONCLUSION

In this paper, we implemented an accurate method of numerically solving the time-dependent Schrödinger equation by using the Numerov formula. We also demonstrated the usefulness of transparent boundary conditions, which allowed the propagation of the wave-function without spurious reflections from the endpoints of the domain.

ACKNOWLEDGEMENT

The financial support of the University of Malaya is gratefully acknowledged.

REFERENCES

[1] Curt A. Moyer, "Numerov extension of transparent boundary conditions for the Schrödinger equation in one dimension", Am. J. Phys., **72**, 351-358 (2004).

[2] A. Goldberg, H. M. Schey and J. L. Schwartz, "Computer-generated motion pictures of one-dimensional quantum-mechanical transmission and reflection phenomena", Am. J. Phys., **35**, 177-186 (1967).

[3] J. Crank J. and P. Nicolson, "A practical method for numerical evaluation of solutions of partial differential equations of the heat-conduction type", Proc. Cambridge Philos. Soc., **43**, 50-67 (1947).

[4] C. N. Veenstra, W. van Dijk, D. W. L. Sprung and J. Martorell, "Time dependence of transmission in semiconductor superlattices", cond-mat/0411118 v3 preprint, Cornell arXiv (2006).

[5] M. Ehrhardt, "Discrete transparent boundary conditions for general Schrödinger-type equations", VLSI Design, **9**, 325-338 (1999).

[6] M. Ehrhardt and A. Arnold, "Discrete transparent boundary conditions for the Schrödinger equation", Rev. di Matem. Della Univ. di Parma, **6/4,** 57-108 (2001).

[7] A. Arnold, M. Ehrhardt and I. Sofronov, "Discrete transparent boundary conditions for the Schrödinger equation: fast calculation, approximation, and stability", Comm. Math. Sci., **1**, 501-556 (2003).